# Progress on waveguide-based holographic video (Invited Paper)

**S. McLaughlin[1], C. Leach[1], S. Gneiting[1], V. M. Bove, Jr.[2], S. Jolly[2], and D. E. Smalley[2,*]**

[1]*Electroholography Group, Brigham Young University, 459 Clyde Building, Provo, Utah 84602, USA*
[2]*MIT Media Laboratory, Massachusetts Institute of Technology, 77 Mass. Ave, Cambridge, Massachusetts 02139, USA*
**Corresponding author: smalley@byu.edu*

Received September 18, 2015; accepted November 26, 2015; posted online January 25, 2016

This paper presents progress on the characterization of guided-wave light modulators for use in a low-cost holographic video monitor based on the MIT scanned-aperture architecture. A custom-built characterization apparatus was used to study device bandwidth, RGB operation, and linearity in an effort to identify optimal parameters for high bandwidth, GPU-driven, full-color holographic display.

*OCIS codes: 090.1705, 090.1970, 090.2870, 090.2890, 090.5694.*
*doi: 10.3788/COL201614.010003.*

Scanned aperture technology was first introduced as a solution for holographic video by the Spatial Imaging Group at the Massachusetts Institute of Technology (MIT)[1]. The MIT architecture uses an acousto-optic modulator (AOM) to create holographic patterns made of acoustic waveforms. As shown in Fig. 1(a), the AOM is imaged through a telescope to demagnify the acoustic waveform. The resulting image has a small apparent lateral extent but a larger angular sweep. A rotating mirror is placed at the Fourier plane of the telescope, which descans the aperture of the AOM to make the travelling acoustic pattern appear stationary and to greatly increase the lateral extent of the display output. This architecture is scaled by adding AOM channels, which increases the overall display bandwidth[2]. Once this is done, the bandwidth can be used to achieve the design parameters of the telescope and the scanning mirror. Furthermore, the display can employ this available bandwidth to increase the display output angle, frame rate, image extent, and vertical resolution[3]. The first two scanned aperture holographic video prototypes were limited in their reproducibility due to the cost of the optical and computational components as well as by the limited bandwidth available from commercial tellurium dioxide Bragg cell AOMs. In his Ph.D. thesis, Dr. St-Hilaire suggested several improvements to reduce cost and increase bandwidth, which included replacing the large doublet output lens with a reflective optic and replacing the tellurium dioxide modulator with a lithium niobate modulator, which has a lower acoustic attenuation and is capable of higher bandwidths than the former. It was assumed, correctly, that the rapid increase in computational power would eventually obviate the need for a costly custom-drive computer[4].

The supercomputer used to run the original prototypes was replaced by Bove *et al.* by a commodity computer utilizing multiple high-end graphics cards[5,6]. Later, many of the expensive optical components, such as the output lens, were replaced with less expensive optics[3]. The optical path was folded to create a display with a monitor-like form factor [see Fig. 1(b)]. The new monitor design was built to include three decks that are folded from water jet cut pieces of aluminum (alloy 5250). The entire optical assembly was made to slide in and out of the display to make it easier to repair and modify the display's optics. The output lens was replaced with a parabolic reflector, rather than a refractive lens. In this way, one is able to construct output optics with smaller f-numbers. This higher numerical aperture at the output enables the focal lengths of the telescope to be shortened while maintaining the total system magnification. This results in a reduced Fourier plane that enables the use of polygons with both fewer and smaller facets.

Smalley and colleagues also created a custom guided-wave modulator, fabricated on a lithium niobate substrate, to replace the tellurium dioxide Bragg cell [see

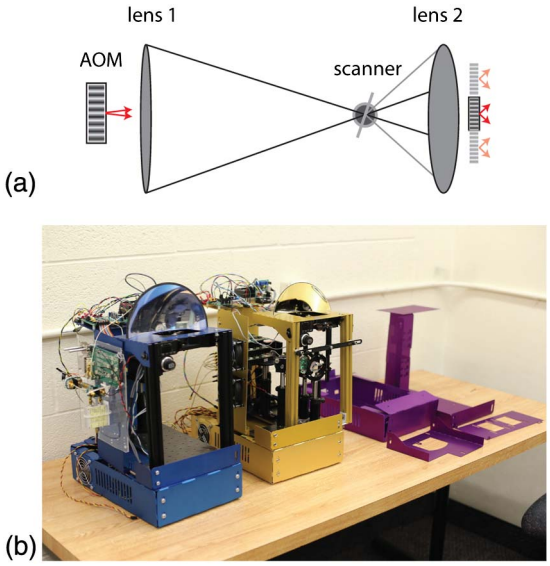


Fig. 1. (a) Scanned aperture holographic video architecture. (b) Holographic video monitors under construction at Brigham Young University.

 

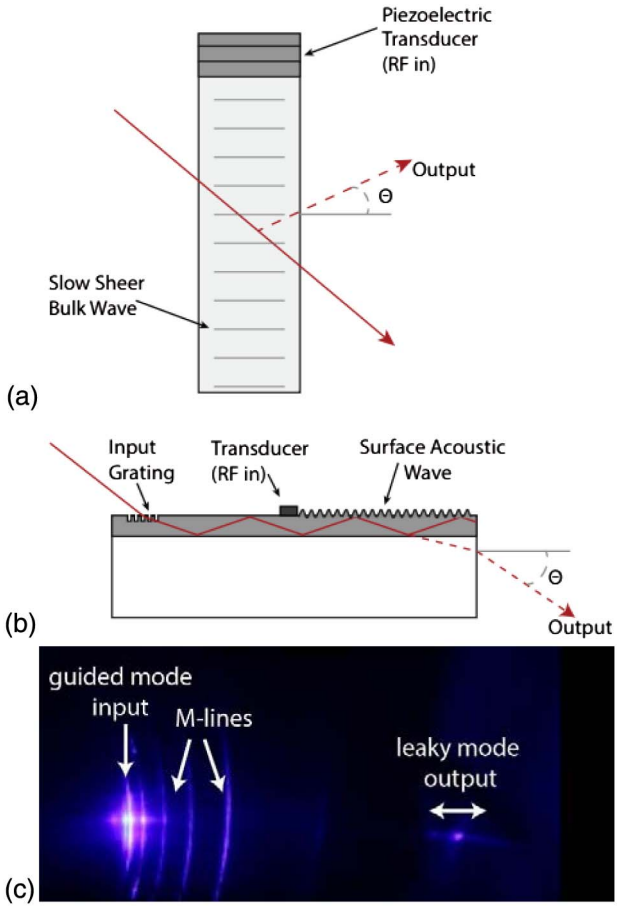


Fig. 2. (a) Bulk wave modulator. A slow sheer wave is emitted from the piezoelectric transducer, which interacts with the input light, deflecting it to Θ. (b) Leaky-mode modulator. Light is coupled into a waveguide, and a SAW is input via a transducer. This interaction deflects the light out of the waveguide at Θ. (c) Output from a leaky-mode device. Light at the left is scattered out of the device from guided modes to form M-lines. The brightest of these lines corresponds to the mode occupied by the input light. To the right is the leaky-mode output light. This light is used to form holographic images. (Scatter was accentuated in this device to make the M-lines more prominent).

Fig. 2(a)]. These changes allowed the overall cost of the display to be reduced by almost two orders of magnitude and the use of guided-wave light modulation made possible future functionality and scalability[7]. In the MIT Mark III prototype these modulators were made to perform the function of both the Bragg cell and the horizontal scanning mirror by utilizing both horizontal deflection within the waveguide device, as well as vertical deflection out of the waveguide via guided to leaky-mode coupling. In this device the vertical scan addressed locations on a helical mirror that served to descan the holographic pattern. This combination of interactions eliminated the need for a large fast polygon or bank of horizontal scanning galvos. However, the quality of descan was limited by the number of scannable points achievable by the guided-wave device. Furthermore, the cascading of these horizontal and vertical scans reduced the total diffraction efficiency and limited the practical achievable image bandwidth of a single modulator to approximately 1 billion pixels per second. When the horizontal and vertical functions were separated, much greater aggregate bandwidths were achievable. When reflective optics made it possible to use small, relatively inexpensive, polygon scanners it was no longer necessary to integrate descan into the AOM. Instead of cascading Bragg deflection and mode coupling, modulators in the Mark IV and following geometries used arrays of single-axis mode coupling channels [see Fig. 2(b)]. These channels could be packed tens of μm apart and each channel could modulate the acoustic equivalent of 100 and 400 million pixels per second. Tight channel packing allowed for the possibility of monolithic devices with aggregate bandwidths in excess of 50 billion pixels per second. It also allowed the use of x-cut lithium niobate rather than z-cut lithium niobate. Cascaded 2D light deflectors used z-cut lithium niobate because a light in the waveguide sees the same material index regardless of its direction of propagation. Unfortunately, z-cut lithium niobate is much less efficient at producing surface acoustic waves (SAWs) than x- or y-cut lithium niobate. This is because the z-cut, x-propagating electromechanical coupling coefficient is lower than the x-cut, y-propagating electromechanical coupling coefficient ($0.53 \times 10^{-2}$ to $3.58 \times 10^{-2}$, respectively)[8].

The guided to leaky-mode interaction provides a number of mechanisms for extracting noise from diffracted light. The guided to leaky-mode interaction can be used to convert transverse electric (TE) guided light into transverse magnetic (TM) polarized leaky-mode light. A polarizer can then be used to separate diffracted light from all other light in the system. Furthermore, the leaky-mode light escapes the confines of the waveguide and is angularly separated from the undiffracted or zero-order light, which remains trapped in the waveguide [see Fig. 2(c)]. This angle of separation is large thanks to the near-collinear illumination.

The near-collinear illumination of the SAW pattern in the waveguide results in a much larger diffraction angle than is possible at near-normal incidence. This is a result of the nonlinear nature of the grating equation

$$\sin \theta_{\text{out}} - \sin \theta_{\text{in}} = \frac{m\lambda}{P},$$

where $\Theta_{\text{out}}$ is the diffracted output angle, $\Theta_{\text{in}}$ is the illumination angle, $m$ is the order of diffraction, $\lambda$ is the illumination wavelength, and $P$ is the grating period. For a given grating period, the change in the diffracted output angle gets larger as the illumination of the grating moves from normal incidence to glancing, or collinear, incidence. It is as if the foreshortening of the grating presents an effectively smaller grating period. The result is that light travelling in a waveguide illuminates the SAW grating and near-collinear incidence and is then diffracted at an angle that may be increased two or three fold. This

increase is further magnified as the light exits the high-index lithium niobate and enters air. This allows the creation of multichannel modulators with much larger diffraction angles than bulk AOMs with similar grating periods.

Multichannel guide to leaky-mode modulators have other advantages over tellurium dioxide with respect to holographic video display. Tellurium dioxide, slow shear mode, Bragg cell AOMs can produce efficient, high-angle deflection thanks to their low acoustic wave speed and good acousto-optic properties, but they suffer from high acoustic attenuation when compared to lithium niobate, which prevents them from operating effectively beyond 100 MHz[9,10]. Lithium niobate has a much lower acoustic attenuation, which allows for the practical use of acoustic frequencies beyond 1 GHz and makes large acoustic bandwidths possible[11,12]. If using SAWs, lithium niobate may also produce lower-cost modulators than tellurium dioxide, in part because tellurium dioxide Bragg cells do not lend themselves to standard wafer-based fabrication processes.

The transducers that produce SAWs can be formed by standard photolithographic processes. The fabrication of these devices is described in Ref. [7].

The author and his colleagues have created an apparatus for the semi-automatic characterization of guided-wave devices[13]. This apparatus operates as shown in Fig. 3(a). The radio frequency (RF) input to the SAW transducer is swept over a range of frequencies, and the corresponding diffracted output is swept over a set of output angles. For each frequency sweep the output power is recorded at one angular position by a photodetector, which is stepped gradually in order to sample a range of possible output angles. The resulting data form a graph of output power as a function of input frequency and output angle. This information provides a "data map" like the one shown in Fig. 3(b) that makes it possible, at a glance, to determine the center frequency, approximate bandwidth, linearity, and point spread of the guided-wave modulator's output light. The frequency response of the device is given by the $x$ axis projection and the angular response is given by the $y$ axis projection. A data map is made for one color at a time, but these maps can be superimposed to show the response for red, green, blue systems.

The reader will note that the data map contains several "islands" of optical output power. These islands correspond to specific guided to leaky-mode transitions in the device. Light entering the device travels in a discrete waveguide mode. Later, when it interacts with the SAW, this guided-mode light is converted to leaky-mode light. Each of these islands represents one of these guided to leaky-mode transitions.

These transitions can be modified by changing the waveguide parameters, such as the depth and index gradient profile. These changes affect the supported modes for a given wavelength of light in the waveguide. Light confined to a given mode has a certain momentum, represented by its wavenumber. Likewise, the SAW interacting

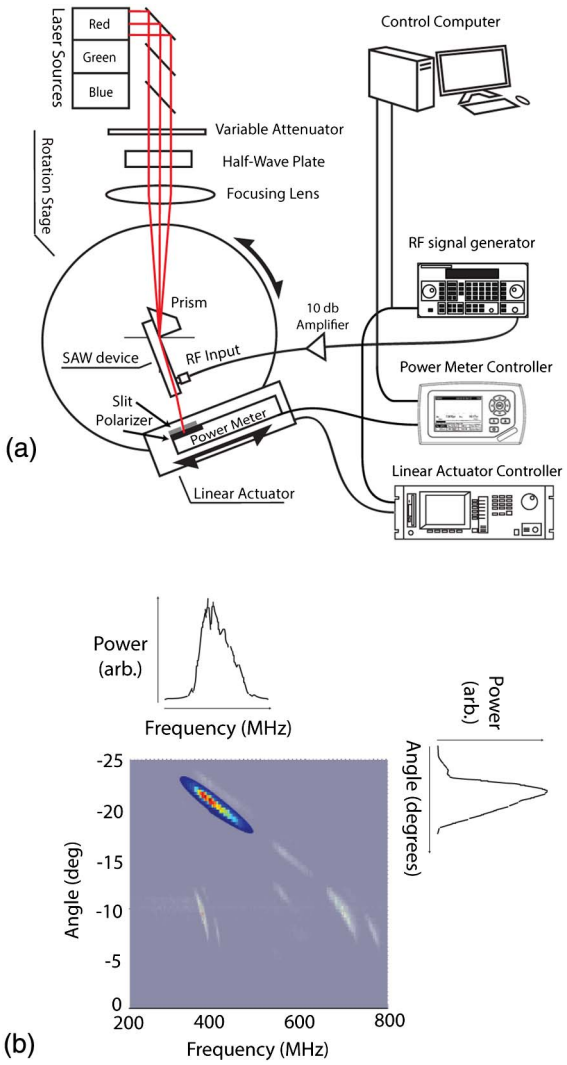


Fig. 3. (a) Semi-automatic characterization apparatus. For each step of the power meter the RF input frequency is swept and the resulting graph formed by this data is referred to in this paper as a "data map". (b) Example of a data map. Note that the data map shows the optical output power of the guided-wave device as a function of both RF drive frequency and output angle. The $x$ axis projection gives the frequency response and the $y$ axis projection gives the angular output.

with the light also has momentum. These momentums undergo vector addition, resulting in a loss of forward horizontal momentum in the mode of light. As a result, the mode is no longer confined to the waveguide and leaks out into the bulk substrate.

The angle of the propagation of the leaky-mode output light is directly related to the momentum of the SAW. By varying the frequency of the SAW the output light can be scanned or shaped. This leaky-mode output has both an RF and angular bandwidth that appears as an island on the data map.

By characterizing a number of samples using this apparatus, the authors were able to identify a device with a shallow waveguide capable of the frequency control of color[14]. For this device, the acoustic frequency response

of red, green, and blue light is separated, but the output of these colors can be made to overlap. This makes it possible to modulate red, green, and blue light in a holographic display simply by changing the frequency content of the input signal, obviating the need for a color filter wheel or dedicated red, green, and blue channels.

Further testing showed that the bandwidth and center of the output frequency response could be manipulated by adjusting the waveguide parameters, such as depth, profile, and index of refraction (see Figs. 4(a) and 4(b)). This made possible the optimization of a device that had adjacent red, green, and blue frequency responses that fit within a 200 MHz envelope [Fig. 4(c)]. A single channel of this device is now matched to the bandwidth of a single GPU output, which makes driving multiple channels on this device both straightforward and highly parallel[14].

The characterization apparatus is now being used to study other optimization criteria of interest, including linearity and slope. Data maps like the one shown in Fig. 5(a) reveal nonlinearities in the device outputs at angles that are nearly parallel with the plane of the device. This nonlinearity arises from the fact that the grating equation that governs diffraction from this surface is not linear, but rather hyperbolic. The effect of this nonlinearity on the optical output is shown in Fig. 5(b). The RF input to the device is being stepped in uniform increments of 6 MHz, but the deflection of the output is not uniform; instead, there is less deflection at low frequencies and more at higher ones. This nonlinearity is undesirable because it will require a software filter to correct; however, it is tempting to use this transition to take advantage of the larger deflections available in the nonlinear region. Ideally, one would like to have

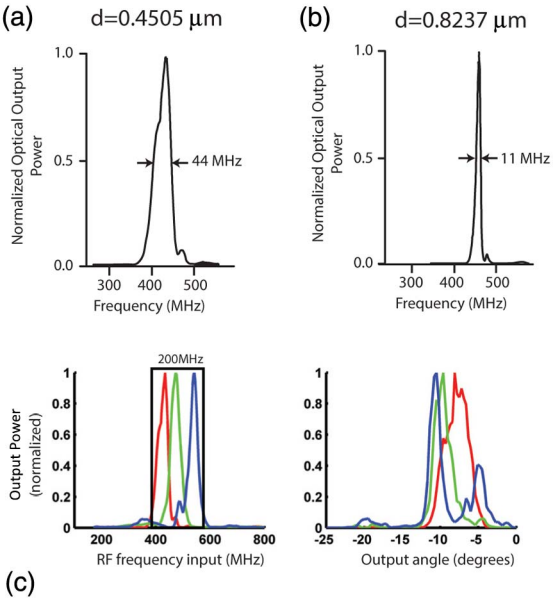


Fig. 4. (a) Frequency response for a guided-wave device with a shallow waveguide, (b) frequency response for a guided-wave device with a deep waveguide, and (c) frequency and angular response of a guided-wave device optimized for the frequency control of color.

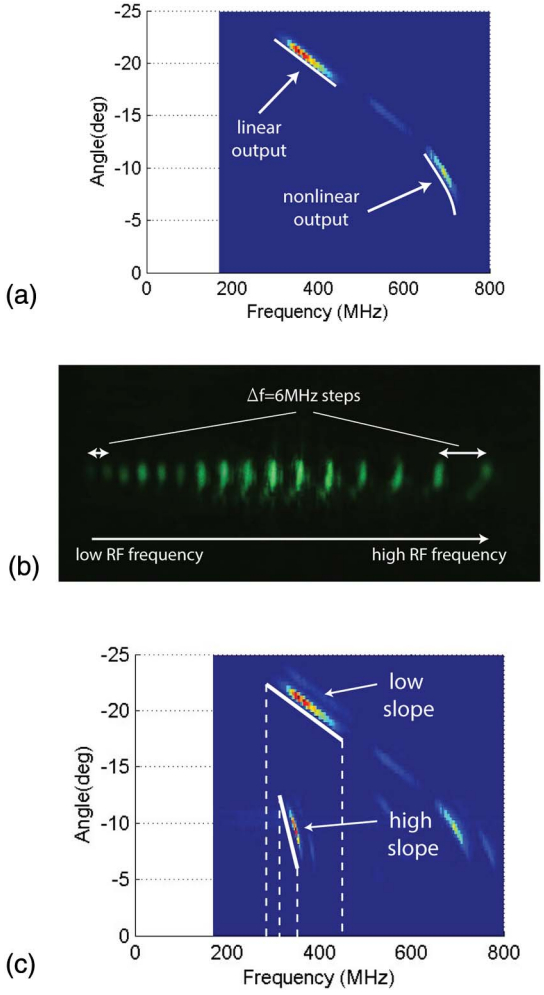


Fig. 5. (a) Data map showing both nonlinear and linear outputs. (b) An image showing the composite output of a nonlinear transition as the RF input is swept from low frequency to high frequency in 6 MHz steps [an example of this type of transition is shown in the right part of (a)]. If the transition were linear, these spots would be separated uniformly. However, this transition is nonlinear, so we see a variation in deflection angle at high frequencies even though the frequency step is constant. (c) A data map showing output with both low and high slopes. Note that the both outputs cover a similar range of angles, but in the case of the high slope output this range is controlled by a much smaller RF bandwidth. One can chose the high or low slope transition, as desired, by modifying the launch conditions (input angle) of the illumination light at the input.

both high angular deflection and linear behavior. The data map in Fig. 5(c) shows such a transition. The higher slope of the lower transition corresponds to a high ratio of angular deflection to input frequency. The authors are in the process of exploring the possible tradeoffs of using these high-slope transitions that may impact, for example, the effective numerical aperture of the deflected light.

The characterization of guided-wave devices has made it possible to begin optimizing these devices for low-cost holographic video display. Using a custom-built characterization device, the authors have optimized the frequency control of color and bandwidth. They have used

data maps to match aggregate device bandwidth to that of common GPU signals. The authors have identified transitions with both nonlinear and linear responses and are examining transitions with the potential for large angular deflections controlled by relatively small RF bandwidths.

As part of a future work, guided-wave devices may be optimized for other criteria important to holographic display, such as diffraction efficiency and point spread function. Data maps, such as those shown above, will continue to be important as these criteria are evaluated.

Future work will also include improving the function of input coupling gratings and exploring alternative device fabrication processes with the goal of increasing process throughput and yield. Now that optimal transducer parameters have been identified for RGB operation, it is desirable to eliminate the direct write step in the fabrication of transducers for guided-wave devices. The minimum feature size for the transducers is over 1 μm and it should be possible to pattern these transducers by photolithography. Such a process would involve first photolithographically patterning aluminum transducers, then covering the wafer and transducers with silicon nitride or silicon dioxide, and then patterning and proton exchanging waveguides. After the oxide or nitride is stripped, an intact wafer of devices should remain. Such a process would greatly increase device throughput. Also, using an expensive rutile prism to couple light into the guided-wave devices defeats the purpose of having created low-cost light modulators. The prisms could be replaced by grating input couplers.

It would be desirable to investigate how to best reduce cross talk between guided-wave channels to allow for the tightest possible channel packing in the light modulation devices. The authors would also like to investigate the effect of other proton exchange techniques on the quality of guided-wave devices.

Finally, new graphics cards are rapidly moving away from fast analog outputs toward greater numbers of digital outputs. It soon will be necessary to identify a driving scheme that can convert these digital signals to an analog holographic signal at low cost.

With each new optimization, guided-wave devices become better adapted to the challenges of scanned aperture holographic video. The work to date continues to suggest that these modulators have the potential to greatly broaden participation in holographic video by making available a low-cost approach to electroholographic display.

This work was supported by the Air Force Research Laboratory contract FA8650-14-C-6571.

## References

1. P. S. Hilaire, S. A. Benton, and M. Lucente, J. Opt. Soc. Am. A **9**, 1969 (1992).
2. P. St-Hilaire, Opt. Eng. **34**, 2900 (1995).
3. D. Smalley, Q. Smithwick, J. Barabas, V. M. Bove, Jr., S. Jolly, and C. DellaSilva, J. Phys. Conf. Ser. **415**, 012055 (2013).
4. P. St.-Hilaire, "Scalable Architectures for Holographic Video," PhD Dissertation, MIT (1988).
5. V. M. Bove, W. J. Plesniak, T. Quentmeyer, and J. Barabas, Proc. SPIE **5664**, 255 (2005).
6. J. A. Watlington, M. Lucente, C. J. Sparrell, V. M. Bove, Jr., and I. Tamitani, Proc. SPIE **2406**, 172 (1995).
7. D. E. Smalley, Q. Y. Smithwick, V. M. Bove, Jr., J. Barabas, and S. Jolly, Nature **498**, 313 (2013).
8. D. Ciplys and R. Rimeika, Ultragarsas (Ultrasound) **33**, 14 (2014).
9. D. R. Pape, in *IEEE Ultrasonics Symposium*, 617 (1999).
10. C. K. Campbell, *Surface Acoustic Wave Devices for Mobile and Wireless Communications* (Academic Press, 1998).
11. J. Poncot, in *IEEE 1991 Ultrasonics Symposium Proceedings*, 563 (1991).
12. I. Chang and S. Lee, in *1983 Ultrasonics Symposium*, 427 (1983).
13. A. Henrie, B. Haymore, and D. E. Smalley, Rev. Sci. Instrum. **86**, 023101 (2015).
14. S. McLaughlin, C. Leach, A. Henrie, and D. E. Smalley, Appl. Opt. **54**, 3732 (2015).